

Assimilating altimetric data into a South China Sea model

Chau-Ron Wu¹ and Ping-Tung Shaw

Department of Marine, Earth and Atmospheric Sciences, North Carolina State University, Raleigh

Shenn-Yu Chao

Horn Point Laboratory, Center for Environmental Science, University of Maryland, Cambridge

Abstract. Sea surface heights from the TOPEX/Poseidon altimeter are assimilated into a three-dimensional primitive equation model to derive the circulation in the South China Sea. With data assimilation the model resolves not only the basin-wide circulation but also a dipole off Vietnam and a low/high feature near the Luzon Strait. Mesoscale features are missing in the simulation without data assimilation because of poor resolution in the wind field and inadequate knowledge of the transport through the Luzon Strait. Compared to the case without data assimilation, data assimilation reduces the root mean square error between the simulated and observed sea surface heights by a factor of 2–3. Circulation derived from data assimilation under climatological conditions is contrasted with that during El Niño. In the normal winter of 1993–1994, flow at 50 m depth is strong and cyclonic. Flow at 900 m depth is cyclonic as well. The deep cyclone persists into the following summer. During the 1994–1995 El Niño winter, features in the flow field at 50 m depth either weaken or disappear, and circulation at 900 m depth is anticyclonic. In the summer of 1995 the dipole and the eastward jet off Vietnam at 50 m depth are missing, and the anticyclonic circulation at 900 m depth persists. Temperature at 65 m shows significant warming from fall 1994 to summer 1995. A weakened flow field and warming in the upper ocean are consistent with findings from earlier El Niño events.

1. Introduction

The South China Sea is the largest marginal sea in southeast Asia with an approximate area of 3.6 million km² (Figure 1). The western shelf area from China to the Sunda Shelf is generally shallower than 100 m, while depths in the central and eastern basin are between 1000 and 5000 m. The Pacific intermediate water enters the deep basin through the Luzon Strait at a sill depth of ~2000 m [Nitani, 1972]. The East Asian monsoon winds, from northeast in winter and southwest in summer, drive the general circulation of the South China Sea. The circulation consists of a cyclonic gyre in winter and a smaller anticyclonic gyre in summer, both intensifying along the western boundary of the basin [Wyrtek, 1961].

Numerical models have provided much information on the basin-wide circulation in recent years. The sea surface elevation and the flow field driven by monthly averaged climatological winds in the simulation of Shaw and Chao [1994] compared favorably with the surface hydrography of Wyrtek [1961] and the ship drift charts of Levitus [1982]. Reversal of currents south of China in winter was simulated by Chao *et al.* [1995]. Chao *et al.* [1996a] studied upwelling in the basin using artificial tracers in a numerical model and identified isolated upwelling areas off Luzon and Vietnam. Chao *et al.* [1996b] modeled the interannual variations of the basin-wide circulation and found warming of the upper ocean during El Niño in the 1980s. Using daily winds and sea surface temperature derived from the National Centers for Environmental Prediction (NCEP)/National Center for Atmospheric Research (NCAR) 40 year reanalysis project [Kalnay *et al.*, 1996], Wu *et al.* [1998] found similar weakening in the flow field during El Niño in the early 1990s.

Some mesoscale features in the South China Sea were identified from observations. Intrusion of the Kuroshio water and upwelling off Luzon were studied using data from hydrographic measurements [Shaw, 1989; Shaw *et*

¹Now at Center for Ocean and Atmospheric Modeling, Institute of Marine Sciences, University of Southern Mississippi, Stennis Space Center.

Copyright 1999 by the American Geophysical Union.

Paper number 1999JC900260.
0148-0227/99/1999JC900260\$09.00

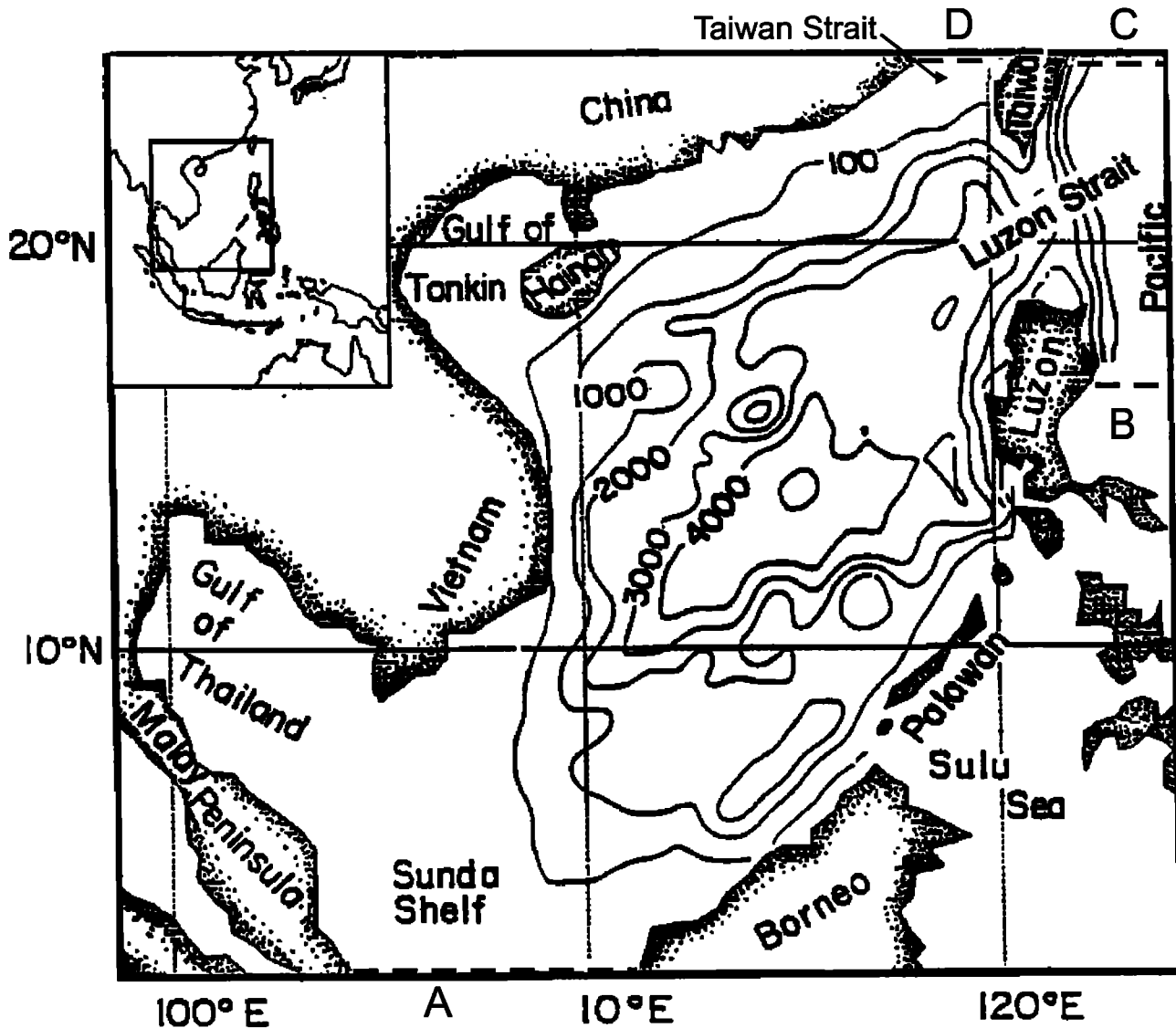


Figure 1. Map of the South China Sea with the 100, 1000, 2000, 3000, and 4000 m isobaths shown. The small insert in the upper left gives the geographical location of the basin. Open boundaries are marked by A, B, C, and D.

al., 1996]. A localized warm pool off Vietnam in spring was observed in the air-dropped expendable bathythermograph (AXBT) data [Chu *et al.*, 1998]. Annual and interannual variations of mesoscale features in the basin were described using sea surface height (SSH) data from the TOPEX/Poseidon (T/P) altimeter [Shaw *et al.*, 1999]. These mesoscale features are generally not well resolved in numerical models. For example, a low in SSH west of Luzon in winter was missing in the numerical simulation of Wu *et al.* [1998]. The model discrepancy is likely due to poor resolution in the wind field (2.5°) and uncertainties in transport estimates through open boundaries.

Circumventing the need for better observations, assimilating the T/P altimeter data into the model of Shaw and Chao [1994] is probably the most promising

method for improving the present description of the circulation in the South China Sea. Assimilating the altimeter data gives a realistic four-dimensional description of the circulation within a dynamical framework. Recent reviews of data assimilation techniques are given by Ghil and Malanotte-Rizzoli [1991] and Haines [1994]. In relatively simple dynamical models, sophisticated methods such as the extended Kalman filter [e.g., Ghil and Malanotte-Rizzoli, 1991] and the adjoint method [e.g., Talagrand and Courtier, 1987] are frequently employed. These methods are computationally intensive in general. From a practical point of view we have chosen simply to insert the altimeter data into the three-dimensional primitive equation model.

Since the SSH is a prognostic variable in the model of Shaw and Chao [1994], the assimilation scheme can

modify the model SSH using the altimeter data without changing the subsurface properties. It is hoped that the numerical model will transmit information downward in some physical or dynamical manner [Holland and Malanotte-Rizzoli, 1989]. However, direct replacement of the SSH by the observed values hardly affects the circulation in our test runs. Fischer *et al.* [1997] found that direct insertion of SSH affects the barotropic flow only, and the injected SSH information is quickly lost in a few time steps. We encountered similar problems and came to the conclusion that a sustainable assimilation of altimeter data requires projecting SSH changes downward to modify the subsurface mass field.

Earlier studies have demonstrated the importance of a projection scheme to propagate surface information to lower layers [Hurlburt *et al.*, 1990]. This procedure is perhaps one of the most difficult problems inherent in using altimeter data. One method is statistical inference, which uses some statistical relationships to derive changes in subsurface properties from sea surface variations. Mellor and Ezer [1991] and Ezer and Mellor [1994] used this method to assimilate observational data in the Gulf Stream with some success. Statistical inference does not work in the South China Sea because few subsurface observations are available for calculating the correlation coefficients.

In this paper a dynamical inference method is used to project the T/P altimeter SSH to changes in subsurface water properties. This method, first proposed by Haines [1991], enforces conservation of subsurface potential vorticity when the SSH is modified. Thus, surface currents are driven by changes in surface potential vorticity. Cooper and Haines [1996] further extrapolated changes in surface heights to those in subsurface water properties, assuming adiabatic vertical displacement in the water column when the surface SSH is changed. They successfully assimilated the SSH data into a 21-level, eddy-resolving, Cox-Bryan general circulation model. In this paper changes in subsurface properties were calculated on the basis of the method of Cooper and Haines [1996]. These values were then incorporated in the model of Shaw and Chao [1994] using a Newtonian relaxation scheme. In this way the SSH data are incorporated into the model slowly and steadily, avoiding the initialization shock commonly encountered in direct insertion techniques. This approach is attractive because it is easy to implement and is computationally efficient in a three-dimensional primitive equation model.

The model is driven by daily winds spanning a 4 year period from January 1, 1993, to December 31, 1996. The assimilated model result in 1993 is compared to those obtained from the concurrent T/P altimeter data and model simulation without data assimilation. The seasonal and interannual variations of the horizontal velocity and temperature fields are described.

2. Description of Data and the Numerical Model

2.1. Altimeter Data

The T/P satellite altimeter has been operating since September 1992. With an absolute accuracy of 4 cm it is the most accurate altimeter system ever launched. The altimeter data used here were provided by the Jet Propulsion Laboratory (JPL). Initial data processing performed at JPL includes the standard correction for atmospheric effects and the removal of a mean sea surface and tides [Callahan, 1994]. The data repeat every 9 days and 22 hours with a spatial resolution of ~ 6 km along each track. Aliases from the first six dominant tidal components were reduced by harmonic analysis [Shaw *et al.*, 1999]. Data were smoothed using the successive correction method of Barnes [Daley, 1991]. The spatial weighting function is $\exp[-2(x/L)^2]$, where x is distance along the track and $L = 1^\circ$; the temporal weighting function is $\exp[-2(t/T)^2]$, where $T = 30$ days. The choice of T is a tradeoff between low-pass filtering of tidal aliases and retaining oscillations at periods longer than 62 days. This timescale is for data processing only and is different from the relaxation timescale of nudging. The smoothed data were interpolated into the model grid (0.4°) with a sampling interval of 10 days. The analysis of the altimeter data is described in detail by Shaw *et al.* [1999].

2.2. Numerical Model

The model of Shaw and Chao [1994] solves the three-dimensional momentum, temperature, and salinity equations with Boussinesq and hydrostatic approximations. It is similar to the general circulation model of Semtner [1974] except for the addition of a free sea surface. The integration domain is from 2° to 24° N and from 99° to 124° E. The horizontal resolution is 0.4° , and there are 21 vertical layers. Time steps are 2160 s for the internal mode and 21.6 s for the external mode.

Open boundaries, marked by A, B, C, and D in Figure 1, are at the Taiwan Strait, the Sunda Shelf, and east of Luzon Strait as those used by Shaw and Chao [1994]. The external mode velocity normal to the boundary U is specified by U_b , Wyrтки's [1961] bimonthly transports (Table 1) divided by the water depth. On the shallow Sunda Shelf and Taiwan Strait, boundaries A and D, $U = U_b$, and the gradient of SSH normal to the boundary is set to zero. At the two deep boundaries B and C east of the Luzon Strait the SSH is prescribed using the altimeter data, and a correction term is added to U_b . If η_m is the model-derived SSH and η_{obs} is the altimeter SSH, the expression for U is

$$U = U_b \pm \epsilon C_0 \frac{\eta_m - \eta_{\text{obs}}}{H}, \quad (1)$$

where $C_0 = (gH)^{1/2}$ is the phase speed of surface grav-

Table 1. Bimonthly Transport in $10^6 \text{ m}^3 \text{ s}^{-1}$ Through the Open Boundaries

Month	Boundary			
	A	B	C	D
February	-3.0	27.0	-24.5	0.5
April	0.0	37.5	-37.5	0.0
June	3.0	32.0	-34.0	-1.0
August	3.0	28.0	-30.5	-0.5
October	-1.0	27.5	-27.0	0.5
December	-3.5	24.5	-21.5	0.5

Values are from *Wyrтки's* [1961] transport estimates slightly adjusted to compensate for the closing of the narrow passages to the Sulu Sea. Positive and negative values represent inflow and outflow, respectively.

ity waves, $\epsilon = 0.1$ is an empirical constant, and H is the water depth. The positive (negative) sign is used in the northern (southern) boundary. The correction term prevents anomalous buildup of SSH near the open boundary and keeps the transport at the observational level. This approach follows that of *Chao et al.* [1996b], except the more accurate altimeter SSH data are used instead of *Wyrтки's* bimonthly estimates. Calculations are not sensitive to the specification of the velocity V tangential to the open boundary. For outflow, V is dictated by advection. For inflow the value upstream of the open boundary is set to zero. A detailed description of the model has been given by *Shaw and Chao* [1994] and *Chao et al.* [1996b].

After being initialized by the January temperature and salinity fields of *Levitus* [1982] the model is spun up by climatological forcing for 1 year. The model is then forced by the NCEP/NCAR daily wind and sea surface temperature (SST) fields beginning on January 1, 1992. Assimilation of the altimeter SSH begins in October 1992, when T/P altimeter data become available. The simulation continues to the end of 1996. The 4 year period from January 1, 1993, to December 31, 1996, is used for analysis.

3. Data Assimilation Scheme

The vertical projection method of *Cooper and Haines* [1996] requires vertical displacements of all isopycnal surfaces in a water column by the same amount Δh when the SSH is changed. Since the vertical displacement is the same, water properties and potential vorticity are not modified except at the surface and bottom. For $\Delta h > 0$ ($\Delta h < 0$), continuity is maintained by removing (adding) light water of thickness Δh at the surface and adding (removing) the same amount of dense water at the bottom. The procedure is applied only in regions with water depths >1000 m. The altimeter data in shallower waters are less reliable; fur-

ther, vertical projection in shallow waters may lead to outcropping of isopycnals.

The displacement Δh is calculated as follows. At each assimilation step, adjusting model SSH (η_m) to altimeter SSH (η_{obs}) results in a surface pressure change $\Delta p_s = \rho_s g (\eta_{\text{obs}} - \eta_m)$, where ρ_s is the mean density of sea water at the surface and g is the gravitational constant. The process of removing light water at the surface and adding dense water at the bottom produces a pressure change $\Delta p_b = \Delta h g (\rho_b - \rho_s)$, where ρ_b is the water density at the bottom. To calculate the vertical displacement, it is necessary to assume that pressure at the bottom is not changed by the adjustment, i.e., $\Delta p_b = -\Delta p_s$, or

$$\Delta h = \frac{\rho_s}{\rho_s - \rho_b} (\eta_{\text{obs}} - \eta_m). \quad (2)$$

The associated changes in temperature and salinity are

$$\Delta T = \frac{\partial T}{\partial z} \Delta h \quad (3)$$

$$\Delta S = \frac{\partial S}{\partial z} \Delta h \quad (4)$$

The vertical derivatives in the above equations are calculated using cubic splines. A convective adjustment follows to remove unstable stratifications.

In this study, ΔT and ΔS are incorporated in the temperature and salinity equations using a Newtonian relaxation scheme [*Anthes*, 1974]. The nudging algorithm to update the model variable $\alpha^m(t)$ to $\alpha^a(t)$ at time t using the observed value $\alpha^{\text{obs}}(t_0)$ at time t_0 is

$$\alpha^a(t) = \alpha^m(t) + KR(t)[\alpha^{\text{obs}}(t_0) - \alpha^m(t)], \quad (5)$$

where K , the nudging coefficient, determines how fast the model results are modified toward the observed value. $R(t)$ is a Gaussian function given by

$$R(t) = \exp[-(t - t_0)^2 / \tau^2], \quad (6)$$

which ramps down from 1 at the time of data injection with an e -folding timescale $\tau = 2$ days. *Holland and Malanotte-Rizzoli* [1989] tested this Gaussian dependence and found that a value of 2 days is most effective. The value of K needs to be large enough to make an impact while being small enough to avoid excitation of gravity waves. *Haltiner and Williams* [1980] suggested that the timescale for K should be smaller than the dominant timescale contained in observations. Tuning leads to $K = 0.015$ in temperature and salinity equations. The corresponding relaxation time is 2 days, which are much shorter than the dominant timescales in the smoothed satellite data.

Updating only the mass field would result in dynamically unbalanced velocity fields. Using a two-layer primitive equation model, *Smedstad and Fox* [1994] showed

the importance of geostrophic correction in data assimilation. *Forbes and Brown* [1996] demonstrated improvements in performance when assimilation is accompanied by a geostrophic correction in the momentum equations. In this paper the barotropic velocities (u and v) are modified in the momentum equations as

$$\frac{\partial u}{\partial t} = (\text{physics}) - \lambda \frac{g}{f} \left(\frac{\partial \eta_{\text{obs}}}{\partial y} - \frac{\partial \eta_m}{\partial y} \right) \quad (7)$$

$$\frac{\partial v}{\partial t} = (\text{physics}) + \lambda \frac{g}{f} \left(\frac{\partial \eta_{\text{obs}}}{\partial x} - \frac{\partial \eta_m}{\partial x} \right) \quad (8)$$

where (physics) represents all conventional terms leading to acceleration, λ is the nudging coefficient, and f is the Coriolis parameter. The terms containing differences between the observed and the model SSH gradients are formulated from the geostrophic relation. Following *Forbes and Brown* [1996], we use $\lambda = 3 \times 10^{-5} \text{ s}^{-1}$, which gives a timescale of ~ 9 hours. A shorter timescale than that in the density equation ensures faster adjustment in the barotropic flow field. The result is not sensitive to the choice of λ .

4. Sea Surface Topography

4.1. Altimeter SSH

The T/P altimeter SSH data in regions deeper than 1000 m are shown in Figure 2 for selected months over a 1 year period in 1993. The February plot shows fragments of the winter low with a weak high developing off central Vietnam. Weakening of the low and strengthening of the high continue in April. The summer circulation begins to develop at the onset of the southwest monsoon; a high appears off Vietnam and another high extends from Luzon westward in June. A fully developed summer circulation pattern is shown on August 8. The high to the north retreats to the coast of Luzon, while the high off Vietnam and a newly developed low to its north form a dipole. The low off Vietnam becomes stronger in October. A fully developed winter pattern appears in December, when low SSHs extend from southeast Vietnam to Luzon with maximum depressions off Luzon and Vietnam.

Variations in the altimeter SSH in the early 1990s have been described by *Shaw et al.* [1999]. Low SSHs over the central basin in winter correspond to a cyclonic basin-wide gyre, while the high off Vietnam in summer indicates a smaller anticyclonic gyre in the southern basin. In addition to these large-scale features, the altimeter data show mesoscale patterns of several hundred kilometers in size. Most noticeable are sea level variations off Luzon and southeast Vietnam. The SSH off Luzon is highest in August and lowest in December. Off Vietnam the SSH is low in December, and high in the early half of the year. A dipole structure appears from August to October. These features are in regions of strong upwelling [*Chao et al.*, 1996a] and are not

resolved in charts derived from historical hydrographic observations.

4.2. Control Experiment

In the control experiment the model was forced by the observed daily wind stress from NCEP/NCAR reanalysis data [*Kalnay et al.*, 1996] without assimilation of the altimeter data. The seasonal patterns in Figure 3 are similar to those by *Wu et al.* [1998]; only a brief description is presented below. In February the SSHs are generally low in the deep basin with the lowest SSH in the northeast and slightly higher SSH in the central basin. The latter develops into a high off Vietnam in April. In June, low SSHs are over shelves to the north and west, and high SSHs are over the deep basin on the southeast side. Low SSHs expand from the Gulf of Tonkin into the deep water south of Hainan in August and are over the deeper part of the northern basin by October. Low SSHs are over the entire deepwater basin in December with the lowest SSHs off Vietnam.

The general features in Figure 3 are consistent with *Wyrtki's* [1961] climatological atlas, but deviate from those in Figure 2 derived from satellite altimeter data in 1993. The winter low in the basin is present in both Figures 2 and 3, but mesoscale features in the SSH field. For example, the highs and lows off Luzon and central Vietnam, are not well resolved, especially when the basin circulation is weak. The discrepancy is likely due to the poor resolution in the wind field. Smoothing and coarse sampling at 2.5° resolution in the NCEP/NCAR data set could not possibly resolve these mesoscale features.

4.3. Experiment With Data Assimilation

The data assimilation experiment is the same as the control experiment, except that the T/P altimeter data were assimilated into the model every 10 days. Figure 4 shows selected snapshots of assimilated SSH patterns. Assimilating the altimeter data produces a high extending from the coast of Vietnam eastward as well as a low off Luzon in February; both are missing in the control experiment but exist in the altimeter SSH field. The two features persist into April. In June the high off Luzon in Figure 2c is well simulated as is the weaker high off Vietnam. The dipole off Vietnam and the high off Luzon in the summer circulation pattern in Figure 2d are reproduced in Figure 4d. The October SSH demonstrates the development of a more compact low off Vietnam than in the case of no data assimilation. In December, two local minima off Vietnam and Luzon in the altimeter SSH in Figure 2f are shown in Figure 4f. In the meantime, only a low is present in the southwest corner of the deep basin in Figure 3f.

Data assimilation could resolve highs and lows off Luzon and Vietnam with spatial scales of several hundred kilometers, but the range of sea level variation in the

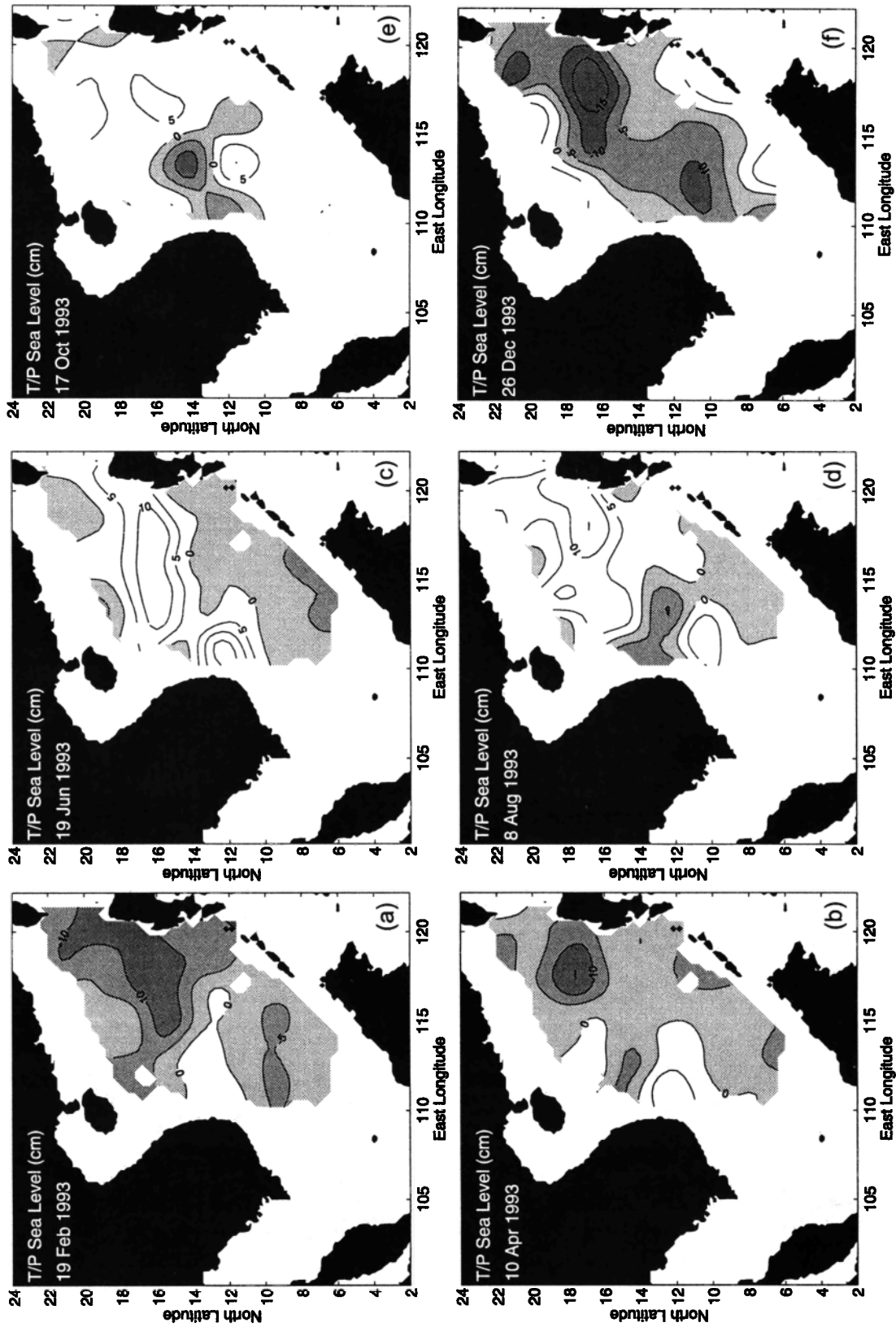


Figure 2. The TOPEX/Poseidon (T/P) sea surface height in 1993: (a) February 19, (b) April 10, (c) June 19, (d) August 8, (e) October 17, and (f) December 26. The contour interval is 5 cm, and negative contours are shaded.

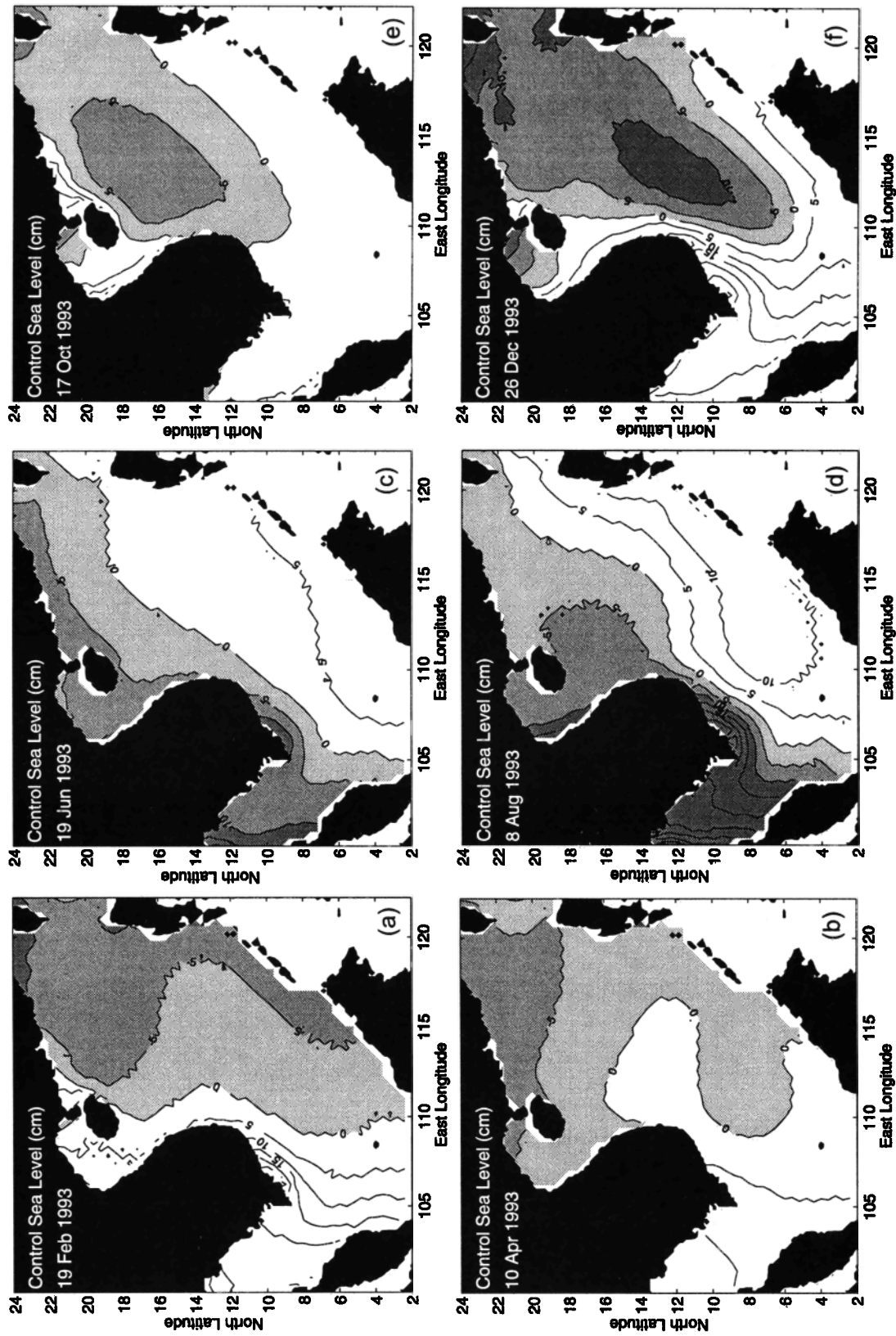


Figure 3. Same as Figure 2 except from the model simulation without data assimilation.

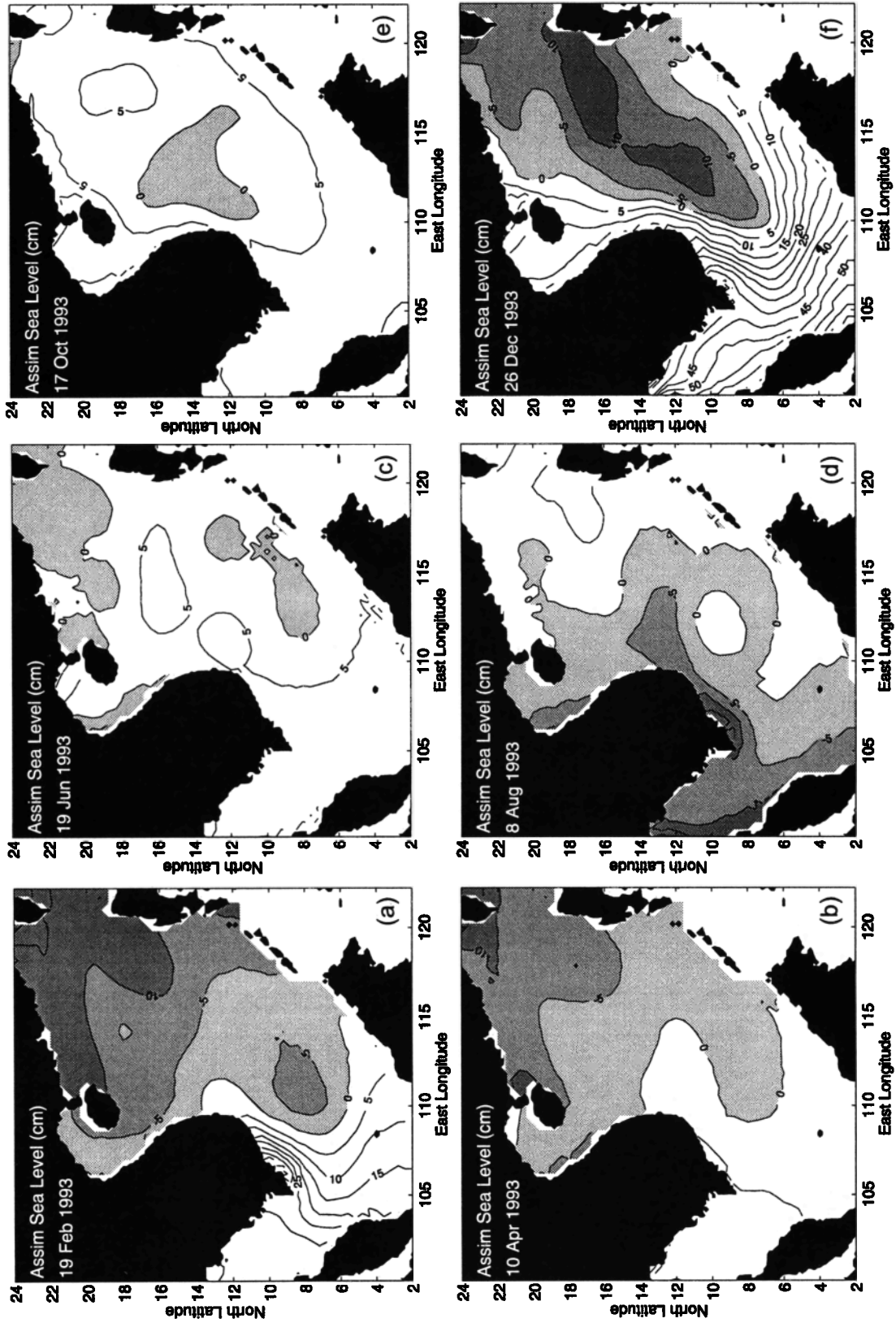


Figure 4. Same as Figure 3 except from the model simulation with data assimilation.

data assimilation experiment is smaller than that contained in the T/P altimeter SSH. It is likely that poor resolution in wind fields in the South China Sea reduces both the intensity and spatial variability of winds [Wu *et al.*, 1998]. Overall, model simulation with data assimilation has improved the SSH field considerably compared to the control experiment without data assimilation.

Quantitatively, the improvement in model simulation can be measured by the root mean square (RMS) error between the model-simulated SSH (η_m^i) and the observed T/P altimeter SSH (η_{obs}^i):

$$RMS = \left(\frac{\sum_{i=1}^N (\eta_m^i - \eta_{obs}^i)^2}{N} \right)^{1/2}, \quad (9)$$

where N is the number of grid points in the assimilation domain (> 1000 m). Figure 5 shows a profound annual cycle in the RMS errors in the control experiment (marked by "W"). Peak RMS errors appear in January-February and in July-August. The error is smaller in transition months (March-April and October-November). It seems that large RMS errors occur in months when the wind-driven currents are strong. However, currents are stronger in winter than in summer, but the RMS error is larger in summer than in winter. Factors other than winds may also contribute to the RMS error. Figure 5 shows that the RMS error is reduced by a factor of 2–3 in the experiment with data assimilation (marked by "A"). Since the observed SSH field is incorporated through temperature and salinity variations, smaller RMS values also demonstrate that

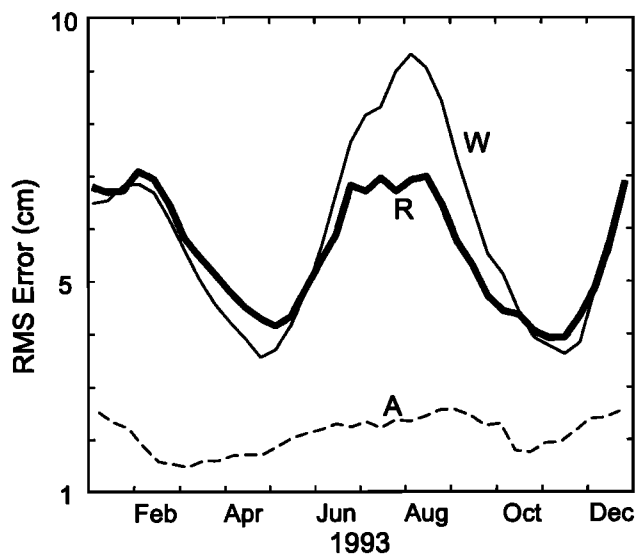


Figure 5. The RMS error in 1993 between the T/P sea surface height (SSH) and model-produced SSH using (a) Wyrтки's [1961] transport estimates without data assimilation (thin solid line W), (b) radiation boundary conditions without data assimilation (thick solid line R), and (c) Wyrтки's estimates with data assimilation (dash line A).

the dynamical approach of projecting sea level information onto the vertical density structure is successful.

As mentioned earlier, depth-integrated transports at the open boundaries are fixed to Wyrтки's [1961] bi-monthly estimates. Specification of the boundary transport is a potential source of the RMS error. To test this idea, we conducted an experiment without data assimilation but using a different open boundary condition for the transport. Instead of Wyrтки's transport estimates, vanishing normal gradients of the barotropic flow are used in the Luzon Strait, Taiwan Strait, and the Sunda Shelf. The resulting RMS error in Figure 5 (marked by "R") is reduced by 30% from the control experiment in summer with little change in other months, suggesting large uncertainties in Wyrтки's transport estimates in summer.

5. Circulation Patterns

5.1. Surface Circulation

Figure 6 shows the circulation pattern in the experiment with data assimilation at a depth of 50 m. The choice of 50 m follows Shaw and Chao [1994]; currents at this depth are representative of the surface circulation of the basin but are not overwhelmed by surface Ekman flow. At the development stage of the winter circulation in October 1993 a boundary current is evident along the coastline from Hainan southward to $\sim 7^\circ\text{N}$, where it turns eastward and northward along Borneo and Palawan. The low in SSH off Vietnam in Figure 2e appears as a cyclonic gyre off Vietnam centered at 14°N , 112°E , consistent with Wyrтки's [1961] observations in October. Currents in the northeastern basin are weak. By December 1993 the boundary current strengthens and extends from Hong Kong southward to the Sunda Shelf. The cyclonic gyre is strongest southeast of Vietnam and over the Sunda Shelf, where the bottom outflow from the Gulf of Thailand is entrained. In the Luzon Strait, surface water enters the South China Sea. In April 1994 a cyclonic gyre is present south of 14°N . In August a tight anticyclone/cyclone pair appears southeast of Vietnam centered by a strong eastward jet leaving the coast of Vietnam between 10° and 12°N . The western boundary current is southward from China to 12°N and northward and into the Gulf of Thailand south 12°N . An eastward jet leaving the coast of Vietnam in summer has been repeatedly reported in historical observations [Wyrтки, 1961], in altimeter SSH [Shaw *et al.*, 1999], and in numerical simulations [Shaw and Chao, 1994]. Trajectories of Argos drifters released recently confirm the existence of such a two-gyre system off Vietnam in summer (J.-H. Hu, personal communication, 1999).

The flow fields obtained from the experiment without data assimilation are shown in Figure 7. In October 1993 the western boundary current off China and northern Vietnam is similar to that in Figure 6a but weakens significantly over the Sunda Shelf, and the cy-

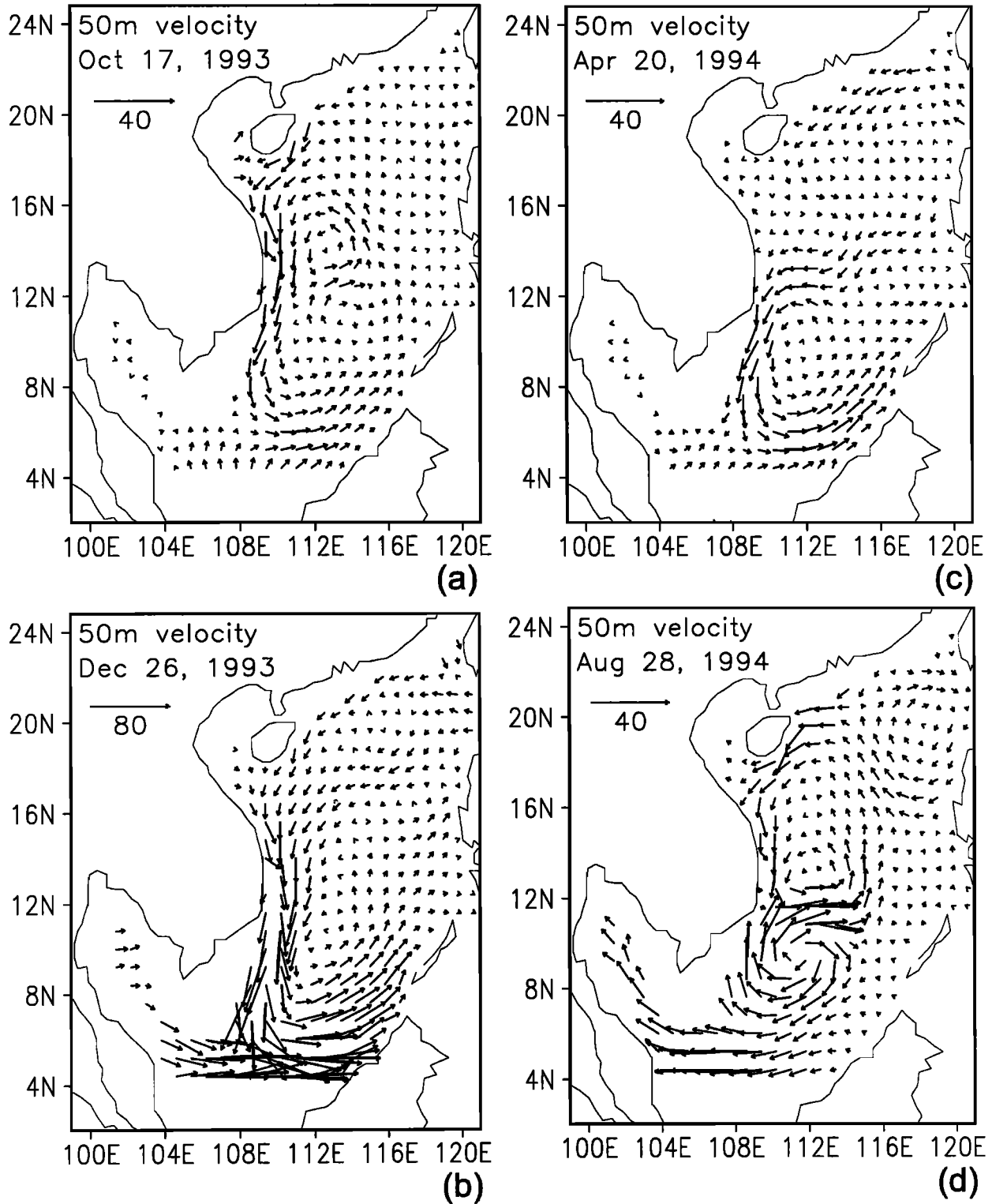


Figure 6. Velocity field at 50 m from the experiment with data assimilation on (a) October 17, 1993, (b) December 26, 1993, (c) April 20, 1994, and (d) August 28, 1994. The velocity scales are in cm s^{-1} .

clonic gyre off central Vietnam is missing. Data assimilation has little effect on the western boundary currents in December, but inflow from the Luzon Strait is much weaker without data assimilation. Large differences between the two experiments appear in April 1994. The cyclonic gyre in Figure 6c is completely missing (Fig-

ure 7c). In August strong flow on the Sunda Shelf is present in both experiments, but the boundary current vanishes north of 12°N in Figure 7d. The tight anticyclone/cyclone pair southeast of Vietnam and the eastward jet are also missing in Figure 7d.

Beyond the seasonal timescale, circulation of the

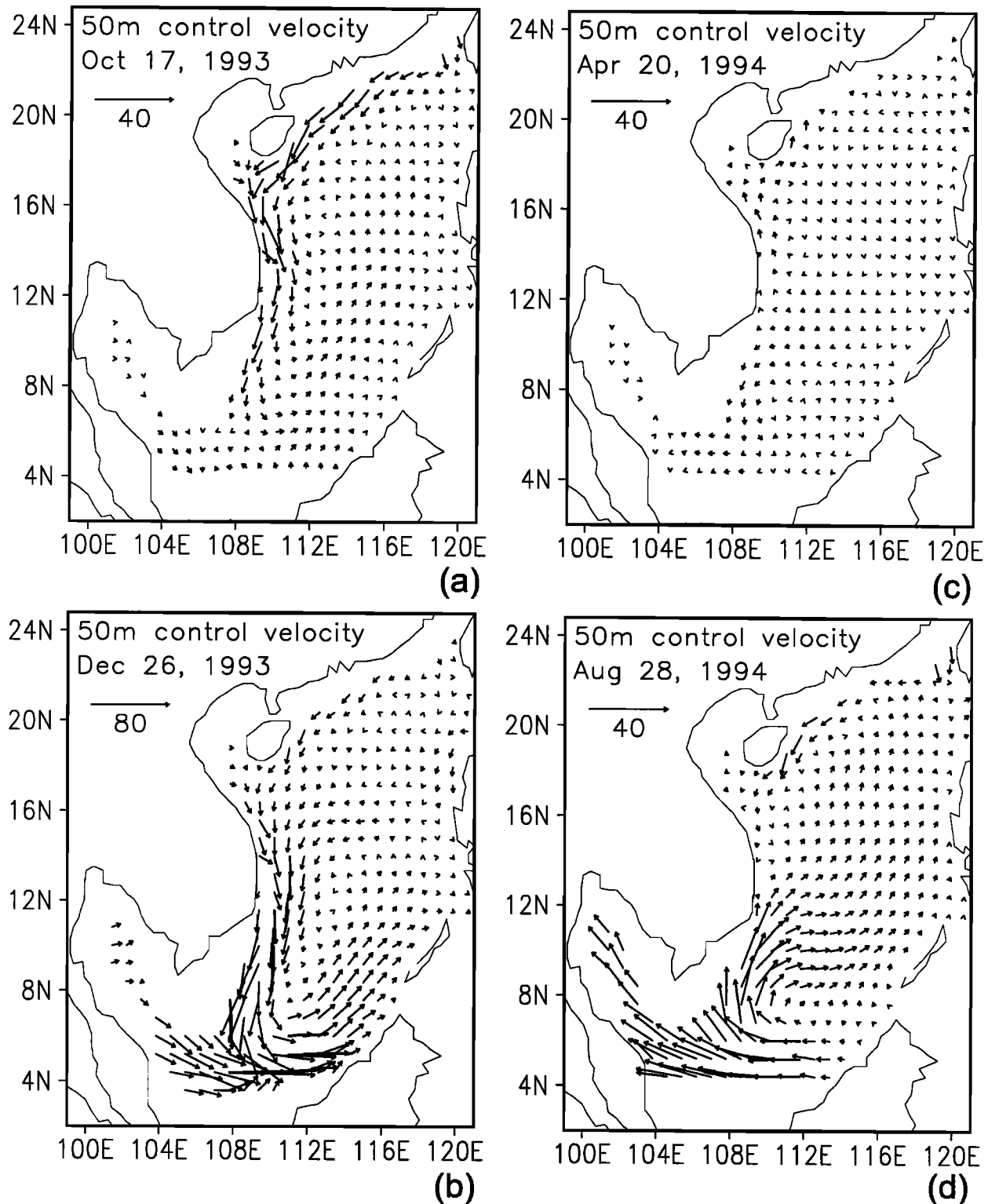


Figure 7. Same as Figure 6 but from the experiment without data assimilation.

South China Sea demonstrates interannual variations. Figure 8, from the experiment with data assimilation, shows the velocity field at 50 m depth in December 1994 and August 1995. This period is known as an El Niño year in the tropical Pacific [Goddard and Graham, 1997]. In December 1994 the western boundary current is southward along the coast of China and Viet-

nam throughout as in December 1993 (Figure 6b) but is much weaker. In the summer of 1995 following the El Niño winter, currents south of Hainan and in the Gulf of Thailand in Figure 8b are similar to those in Figure 6d. However, the eastward jet off Vietnam and the anticyclonic gyre south of it are missing. Weakened circulation under a weak East Asian monsoon during

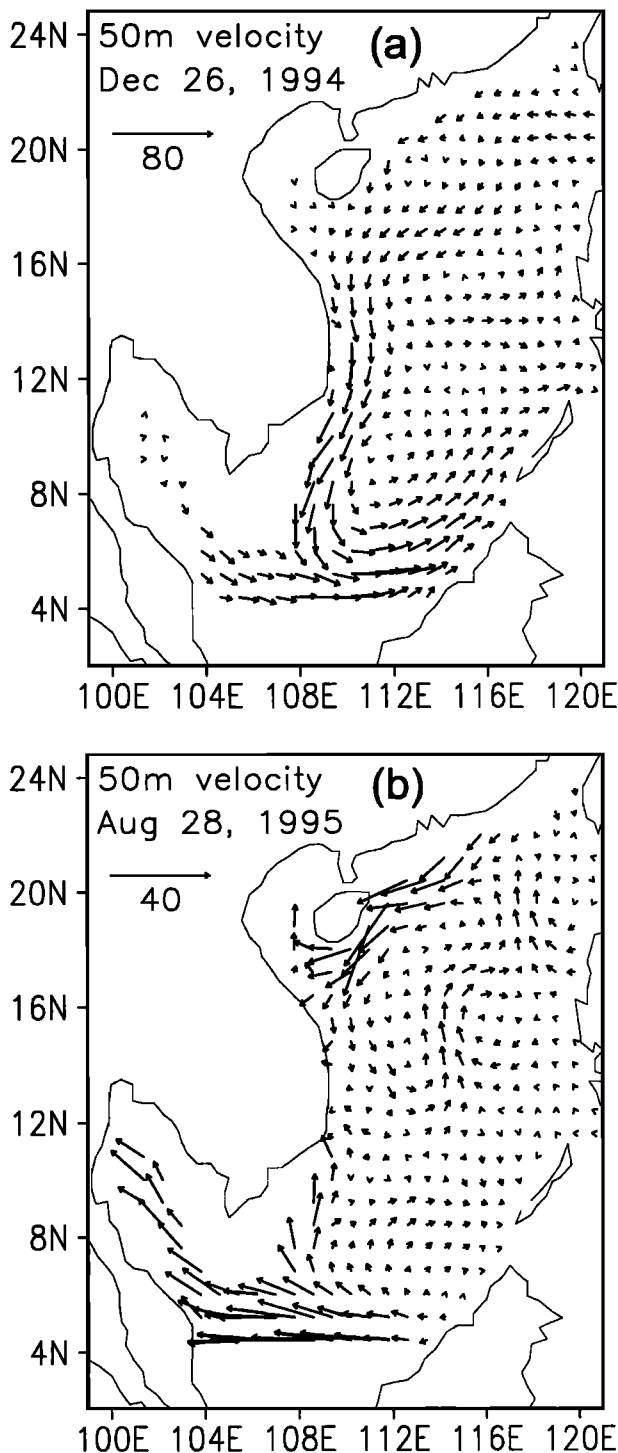


Figure 8. Same as Figure 6 but on (a) December 26, 1994, and (b) August 28, 1995, from the experiment with data assimilation.

El Niño has been reported both in previous numerical experiments [*Chao et al.*, 1996b; *Wu et al.*, 1998] and in observations [*Shaw et al.*, 1999].

5.2. Circulation at 900 m

Currents at 900 m (Figure 9) represent circulation at intermediate depths (from 600 to 1200 m). In December 1993 circulation at 900 m depth is cyclonic. The

gyre, centered at 12°N, 113°E, occupies nearly the entire western half of the deep basin. The deep current along the coast of Vietnam is in the same direction as the surface flow. Except for the flow out of the basin in the Luzon Strait and the anticyclonic flow off Palawan, currents are weak in the eastern basin. The cyclonic circulation in the southern basin persists into summer, producing a southward flow along the coast of Vietnam in the opposite direction of the surface current (Figure 9b). The outflow in the Luzon Strait seems to exist in all seasons. Using pH, alkalinity, and total CO₂ data, *Chen and Huang* [1996] suggested that South China Sea waters flow out of Luzon Strait at depths between 350 and 1350 m. A cyclonic gyre in winter and the year-round outflow at 900 m depth are also given by *Chao et al.* [1996a], but their summer circulation is anticyclonic at 900 m depth [see *Chao et al.*, 1996a, Figure 3]. It is likely that year-to-year variations are present at 900 m.

The flow field in December 1994 (Figure 9c) shows drastic changes in the circulation pattern from that in 1993. Flow becomes northward off Vietnam with a strong current toward northwest off southwest Luzon. The gyre is in the opposite sense of rotation from the previous year. Otherwise, the southwestward flow off Palawan and northern Borneo and the outflow in the Luzon Strait are similar to those in the previous winter. In August 1995 (Figure 9d), currents at 900 m east of Vietnam are in a direction opposite to that in Figure 9b. Flow in the Luzon Strait is also weaker than a year earlier. Note that the surface circulation is weak from late 1994 to summer 1995. It seems that the strong surface cyclonic gyre in a normal winter could penetrate to 900 m depth and could persist into the next summer, but a weak cyclonic surface gyre during an El Niño winter could not reverse the anticyclonic deep circulation. Circulation at intermediate depths in summer seems to always follow that in the previous winter.

6. Temperature Distribution

Upper ocean temperature variations (5, 15, and 25 m depths) in 1993 from the control experiment and the data assimilation experiment are plotted at 12°N, 110.2°E in Figures 10a and 10b. This location is known for summer upwelling in *Wyrtki's* [1961] atlas. Overlaid in the two panels is the surface temperature (0 m) from the NCEP/NCAR data set, which is imposed as a surface boundary condition. The SST increases from <24°C in December to >29°C in May. It drops by ~2°C from May to August, rebounds slightly in September, and decreases thereafter to the December minimum. In the experiment with no data assimilation, temperatures at 15 and 25 m depths do not follow the increase at the surface from February to July, indicating that the surface temperature boundary condition penetrates only the first few meters of the water column. Warming occurs mostly in August. From November to January the top 25 m is well mixed.

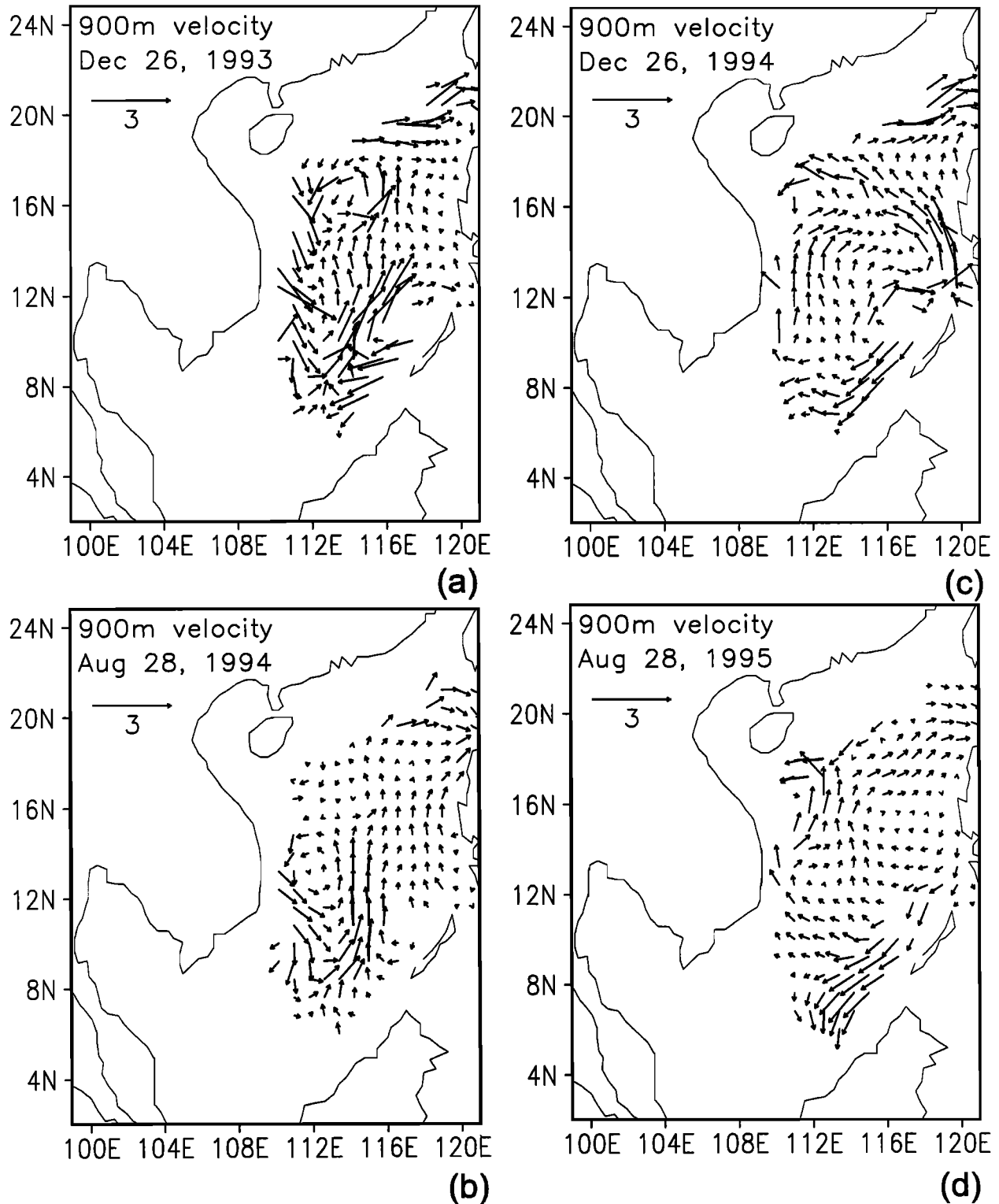


Figure 9. Velocity field at 900 m from the experiment with data assimilation on (a) December 26, 1993, (b) August 28, 1994, (c) December 26, 1994, and (d) August 28, 1995. The velocity scale is 3 cm s^{-1} .

Data assimilation transmits the surface signal to greater depths. From February to July, temperatures at 15 and 25 m follow the variation at surface, reaching a maximum in May. Cooling in July and August reaches both 15 and 25 m depths, indicating that up-

welling is better simulated in the experiment with data assimilation. Figure 10c, from *Levitus and Boyer [1994]*, indicates that the observed seasonal variation of temperature does penetrate to well below 30 m depth. Temperature decreases by 1°C in the top 30 m of the water

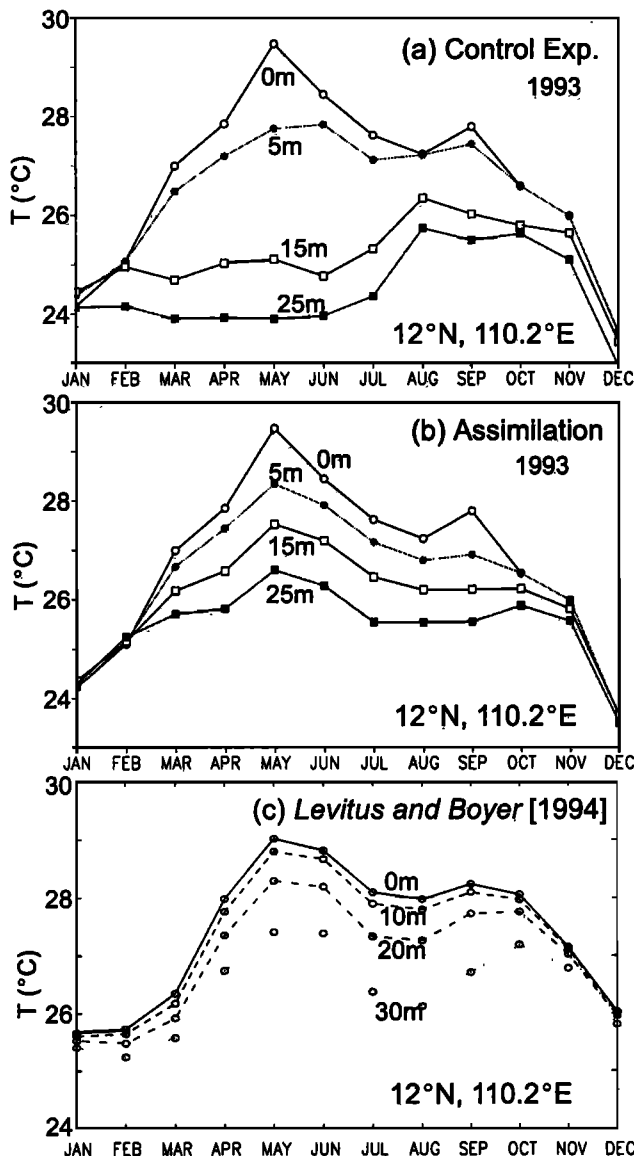


Figure 10. Monthly temperature variations at 5, 15, and 25 m depths at 12°N , 110.2°E in 1993 from the experiments (a) without data assimilation and (b) with data assimilation. The surface values (0 m) is from the National Centers for Environmental Prediction (NCEP)/National Center for Atmospheric Research (NCAR) data set. (c) Temperatures at 0, 10, 20, and 30 m depths at 12.5°N , 110.5°E from *Levitus and Boyer [1994]*.

column in summer at the same location. In the experiment with data assimilation, subsurface temperature is modified directly according to SSH anomalies, indicating that a more realistic temperature field can be obtained by the insertion of altimeter SSH data. Specifying the surface boundary condition in temperature has only little effect on the subsurface field.

It should be noted that SST is specified as the boundary condition; thus only the subsurface temperature field is described in this paper. Differences in subsur-

face temperature between the two experiments along two zonal sections give the depth of penetration of the SSH signal. In summer 1993 (Figure 11a), temperature at 12°N , 110.5°E in the upwelling region off Vietnam is underestimated by 2°C at 65 m depth in the experiment without data assimilation. In December 1993, temperature along 17.2°N in the upwelling region off Luzon [*Shaw et al., 1996*] is similarly underestimated by 2°C at 65 m depth at 118.5°E and by 2°C at 235 m depth at 118°E (Figure 11b). Thus data assimilation could improve the description of temperature variations associated with upwelling in the South China Sea. The horizontal temperature structure at this depth is further described below.

6.1. Period From Late 1993 to Mid 1994

Major features shown in October 1993 are a dipole off Vietnam and a warm tongue extending westward from Luzon Strait to 115°E (Figure 12a). The former is the remnant of the summer feature in the SSH field (Figure 2e). In the Luzon Strait the warm tongue is likely associated with the intrusion of Kuroshio waters; a weak current into the basin through the Luzon Strait can be seen in the velocity field in Figure 6a. Intrusion of the Kuroshio waters in late fall and winter is consistent with observations [*Shaw, 1991*]. In December 1993 two cold water pools, centered at 16°N , 119°E

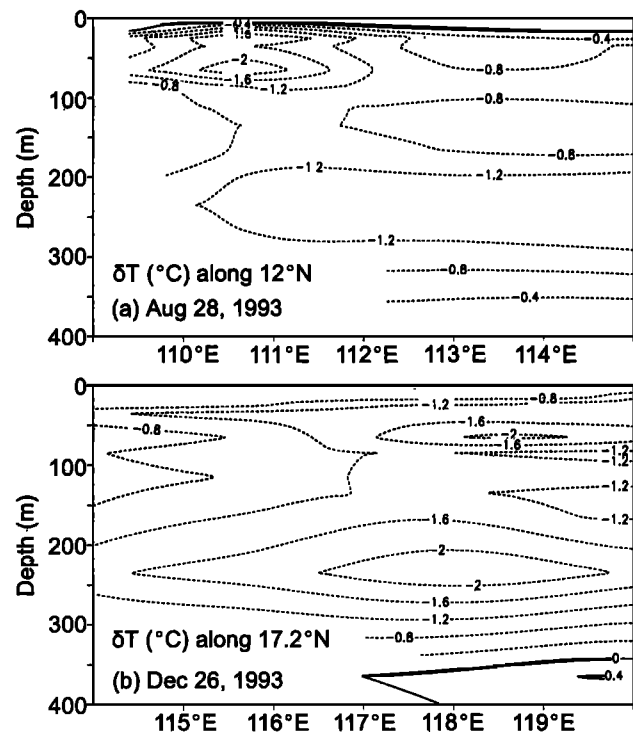


Figure 11. Temperature difference between experiments with and without data assimilation along (a) 12°N on August 28, 1993, and (b) 17.2°N on December 26, 1993. Negative (positive) values indicate underestimating (overestimating) the temperature by the experiment without data assimilation.

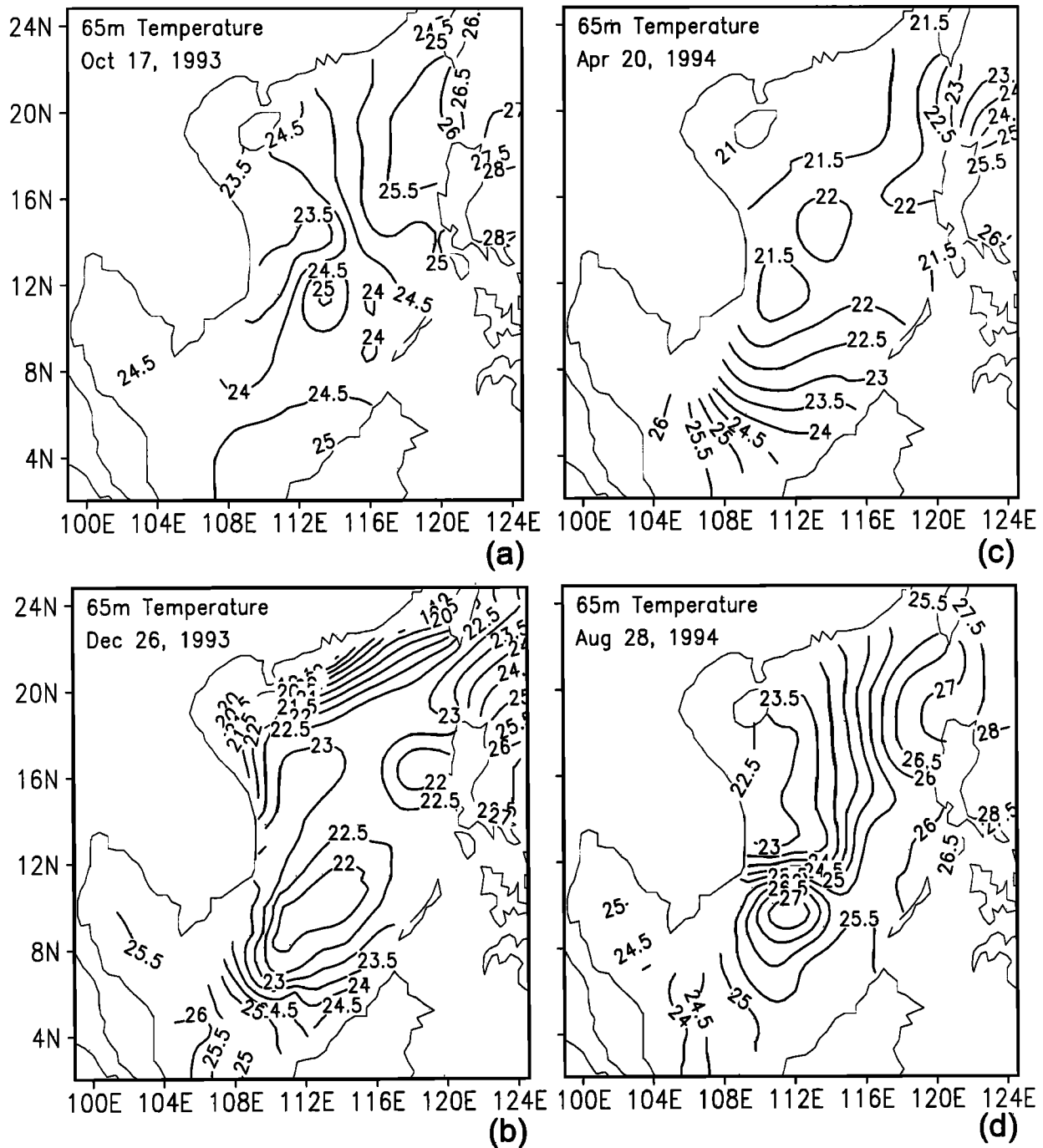


Figure 12. Temperature at 65 m on (a) October 17, 1993, (b) December 26, 1993, (c) April 20, 1994, and (d) August 28, 1994, from the experiment with data assimilation. The contour interval is 0.5°C .

and 10°N , 112°E , appear off Luzon and northern Sunda Shelf with temperature $<22^{\circ}\text{C}$ (Figure 12b). The two cold pools correspond well to the two lows in Figure 2f and are at locations of heat losses exceeding 100 W m^{-2} in *Levitus'* [1984] atlas. The one off Luzon is consistent with the location of winter upwelling [Shaw *et al.*, 1996]. Both cold pools disappear in the following April, and a warm pool seems to develop off Vietnam (Figure 12c). In August with the summer pattern fully developed,

relatively cold water extends from the Gulf of Tonkin into the deep basin, while the highest temperature is located in a warm pool off the Sunda Shelf. The large temperature gradient east of Vietnam corresponds well to the location of the eastward jet in Figure 6d.

6.2. Late 1994 to Mid 1995

Drastic warming occurs in October 1994; the tongue from the Luzon Strait is warmer by $\sim 1^{\circ}\text{C}$ and extends

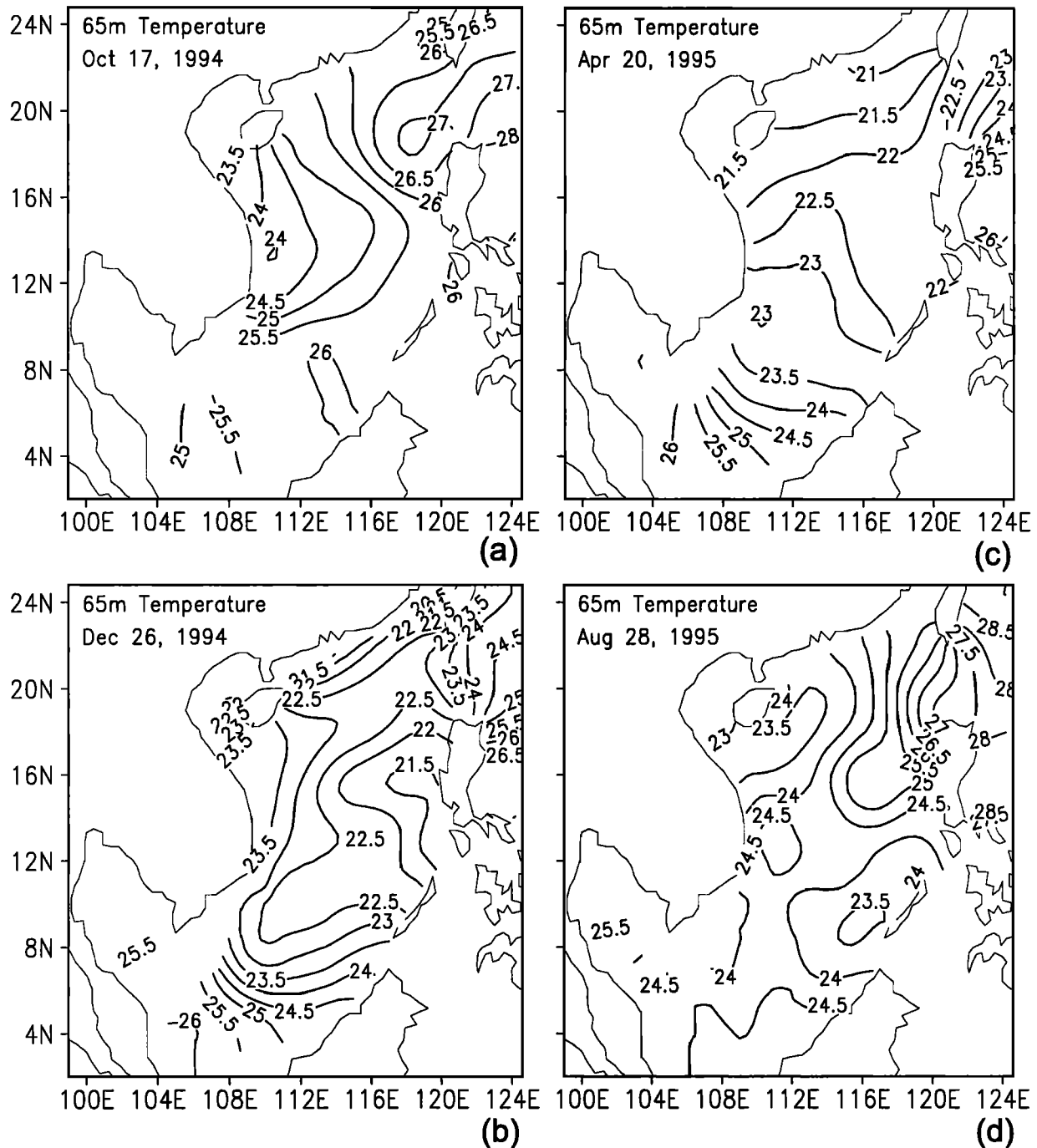


Figure 13. Same as Figure 12 except on (a) December 17, 1994, (b) December 26, 1994, (c) April 20, 1995, and (d) August 28, 1995.

farther westward into the basin than in 1993 (Figure 13a). In fact, the temperature in the entire basin is warmer. The increase in temperature reaches nearly 2°C in the southern basin. Warming in October 1994 persists into December (Figure 13b). Comparing to Figure 12b, significant warming occurs in the coastal waters off China and in the cold pool off Sunda Shelf. However, some cooling southwest of Luzon is noted. Warming in late 1994 persists into the following spring (Figure 13c). In April 1995 warming of 0.5–1.5°C could

be found in the southern basin. A nearly uniform north-south temperature gradient dominates the temperature field, which displays little patchiness. Drastic differences also appear in summer 1995 (Figure 13d). The relatively cold water extending from the Gulf of Tonkin is warmer by 0.5°C than in the previous summer. Also, the warm pool off Vietnam disappears in the summer of 1995.

Warming during an El Niño event in the South China Sea has been well established. The temperature distri-

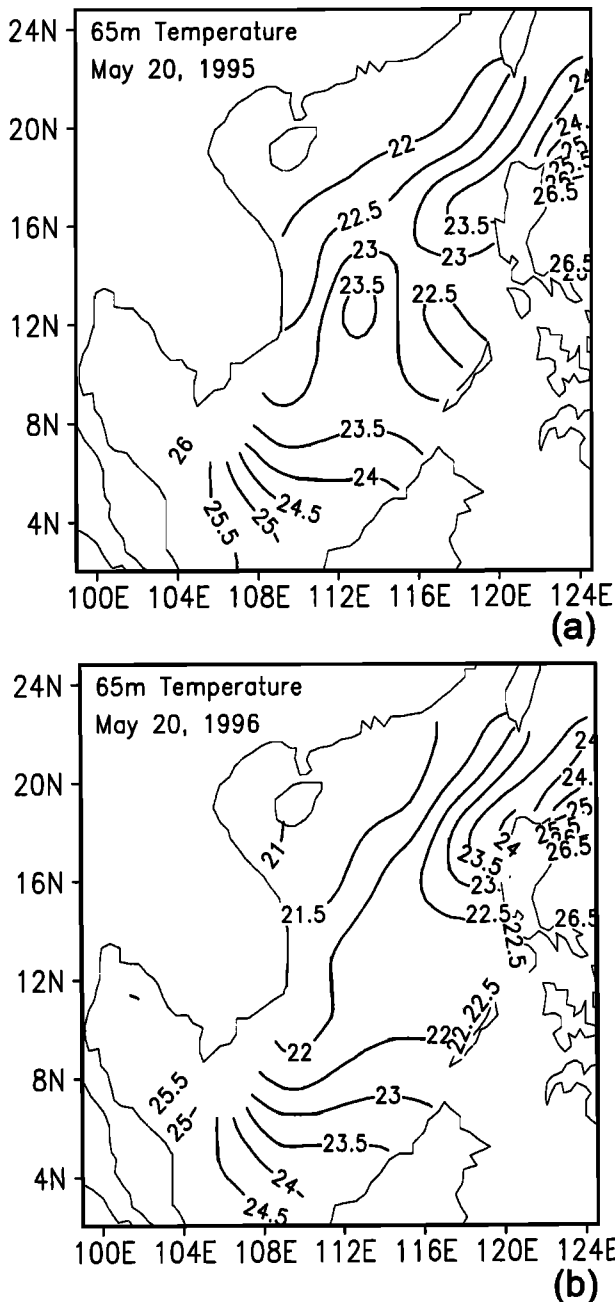


Figure 14. Same as Figure 13 except on (a) May 20, 1995, and (b) May 20, 1996.

bution at 65 m reaffirms earlier findings. It is likely that warming begins in October 1994 after a normal year from late 1993 to mid 1994. Warming is seemingly accomplished by a stronger Kuroshio intrusion in October, smaller temperature contrasts in summer and winter, and disappearance of the dipole in summer. Smaller temperature contrasts suggest weakened winter and summer gyres, consistent with earlier findings.

Another interesting feature, seemingly to occur in spring during a warm event, is a warm water pool off southeast Vietnam. The pool is represented by a local temperature maximum at 65 m on May 20, 1995 (Fig-

ure 14a), indicating possible localized downward advection. Maximum temperature at $12^{\circ}30'N$, $113^{\circ}E$ exceeds $23.5^{\circ}C$. This feature is present only in the data assimilation experiment. Without assimilation, isotherms in the deepwater region are featureless; a uniform north-south temperature gradient is present in the basin (not shown), as in *Levitus and Boyer's* [1994] atlas. In the 4 year period from 1993 to 1996 the warm pool off Vietnam is not always present. For example, it is missing on May 20, 1996 (Figure 14b). AXBT survey between May 14-25, 1995 [Chu *et al.*, 1998, Figure 6] seems to confirm the existence of such a warm pool.

7. Discussion

One important task in assimilating the altimeter data by direct insertion or nudging is to infer subsurface density variations from SSH. The lack of simultaneous spatial and temporal coverage in subsurface oceanographic measurements prevents us from deriving statistical correlation coefficients between surface and subsurface fields in the South China Sea. The dynamical inference method of *Cooper and Haines* [1996] modifies mass fields in the water column through lifting or lowering of isopycnals. Statistical analysis of the conductivity-temperature-depth (CTD) data in the Azores Current by *Gavart and De Mey* [1997] shows that the first empirical orthogonal function (EOF) mode of isopycnal displacement consists of coherent lifting or lowering of isopycnals in the entire water column. The statistical result seems to validate the Cooper and Haines method in some geographical areas.

In carrying out vertical projection it is assumed that there is no pressure change at the bottom. *Drakopoulos et al.* [1997] relaxed the bottom pressure constraint by modifying bottom pressure according to the change in relative vorticity induced by stretching or compression of the water column. Their twin experiments in the Mediterranean show that the result is slightly worse after 100 days of wind forcing than that using the original method of *Cooper and Haines* [1996]. They conclude that this modification may be unnecessary if the correct wind stress is known. Thus using a daily wind field makes it less important to correct the bottom pressure. Another limitation in this paper is that the subsurface mass field is modified only in water deeper than 1000 m. However, motion in the western shelf region may still be modified by data assimilation via model physics. *Fischer and Latif* [1995] found that inserting information in the west Pacific modifies the signal in the east Pacific significantly.

One concern in doing data assimilation is how long the inserted information persists in the model. This question is examined by stopping data assimilation during model integration while maintaining all other forcing. The result shows that the RMS error grows quickly and reaches the value in the control experiment in a month or so (figure not shown), indicating that

the model can retain the SSH information for about a month. Fischer and Latif [1995] found that the memory lasts for a few months in their model assimilation of SST, island-based SSH observations, and subsurface temperature data in the tropical Pacific. The South China Sea is in low latitudes and is not too large in size. Such a short memory is not unreasonable. Since past memory is erased in a short time, assimilating SSH in the South China Sea is useful for the diagnostic purpose instead of forecast.

8. Summary and Conclusions

Data assimilation produces model states that are representative of the observations, yet they are constrained by physics of the numerical model. In this paper, mesoscale variabilities in sea level, velocity, and temperature fields are better resolved than in previous studies. The large RMS error between the simulated SSH and T/P SSH in the experiment without data assimilation indicates inadequate spatial resolution in the NCEP/NCAR winds and uncertainties in Wyrski's [1961] transport estimates in summer. With data assimilation the RMS error is reduced by a factor of 2–3, demonstrating that uncertainties associated with the forcing field and boundary conditions could be remedied to a certain extent by assimilating altimeter data.

During the period studied, warming related to El Niño begins in October 1994 following a normal climatological period from late 1993 to mid 1994. The simulation shows warming of the upper ocean by 1°–2°C and weakening of the circulation gyres during the El Niño winter of 1994–1995. The surface gyre is also weaker in the following summer. A tight dipole structure in both temperature and velocity fields is present off Vietnam in the climatological summers. The dipole structure is missing following a winter of weakened monsoon winds. The result is consistent with earlier findings. Circulation at 900 m depth is cyclonic when the winter gyre at the surface is strong, and the cyclonic circulation persists into the following summer. In a winter with a weak surface gyre, circulation at 900 m depth is anticyclonic in both winter and the following summer. Isolated pools of water in the upwelling areas off Vietnam and Luzon are detected with data assimilation. A new feature identified is a warm water pool off Vietnam in May 1995 detected in an AXBT survey as well.

Acknowledgments. We would like to thank M. Fischer and an anonymous reviewer for suggestions. This research was supported by the National Science Foundation under grants OCE95-02984 to PTS and OCE95-04959 to SYC. The TOPEX/Poseidon altimeter data were kindly provided by Lee-Lueng Fu of the Jet Propulsion Laboratory (JPL). The North Carolina Supercomputing Center provided CPU time on its Cray T90 for the model simulation.

References

- Anthes, D. L. T., Data assimilation and initialization of hurricane-predicting models, *J. Atmos. Sci.*, *31*, 702–719, 1974.
- Callahan, P. S., TOPEX/Poseidon GDR user's handbook, *JPL D-8944*, 81 pp., Jet Propul. Lab., Pasadena, Calif., 1994.
- Chao, S.-Y., P.-T. Shaw, and J. Wang, Wind relaxation as a possible cause of the South China Sea Warm Current, *J. Oceanogr.*, *51*, 111–132, 1995.
- Chao, S.-Y., P.-T. Shaw, and S. Wu, Deep water ventilation in the South China Sea, *Deep Sea Res., Part I*, *43*, 445–466, 1996a.
- Chao, S.-Y., P.-T. Shaw, and S. Wu, El Niño modulation of the South China Sea circulation. *Prog. Oceanogr.*, *38*, 51–93, 1996b.
- Chen, C. T. A., and M. H. Huang, A mid-depth front separating the South China Sea water and the Philippine Sea water, *J. Oceanogr.*, *52*, 17–25, 1996.
- Chu, P. C., C. Fan, C. J. Lozano, and J. L. Kerling, An airborne expendable bathythermograph survey of the South China Sea, May 1995, *J. Geophys. Res.*, *103*, 21,637–21,652, 1998.
- Cooper, M., and K. Haines, Data assimilation with water property conservation, *J. Geophys. Res.*, *101*, 1059–1077, 1996.
- Daley, R., *Atmospheric Data Analysis*, 457 pp., Cambridge Univ. Press, New York, 1991.
- Drakopoulos, P. G., K. Haines, and P. Wu, Altimetric assimilation in a Mediterranean general circulation model, *J. Geophys. Res.*, *102*, 10,509–10,523, 1997.
- Ezer, T., and G. L. Mellor, Continuous assimilation of Geosat altimeter data into a three-dimensional primitive equation Gulf Stream model, *J. Phys. Oceanogr.*, *24*, 832–847, 1994.
- Fischer, M., and M. Latif, Assimilation of temperature and sea level observations into a primitive equation model of the tropic Pacific, *J. Mar. Syst.*, *6*, 31–46, 1995.
- Fischer, M., M. Latif, M. Flugel, and M. Ji, The impact of data assimilation on ENSO simulations and predictions, *Mon. Weather Rev.*, *125*, 819–829, 1997.
- Forbes, C., and O. Brown, Assimilation of sea surface height data into an isopycnic ocean model, *J. Phys. Oceanogr.*, *26*, 1189–1213, 1996.
- Gavart, M., and P. De Mey, Isopycnal EOFs in the Azores Current region: A statistical toll for dynamical analysis and data assimilation, *J. Phys. Oceanogr.*, *27*, 2146–2157, 1997.
- Ghil, M., and P. Malanotte-Rizzoli, Data assimilation in meteorology and oceanography, *Adv. Geophys.*, *33*, pp. 141–266, Academic, San Diego, Calif., 1991.
- Goddard, L., and N. E. Graham, El Niño in the 1990s, *J. Geophys. Res.*, *102*, 10,423–10,436, 1997.
- Haines, K., A direct method for assimilating sea surface height data into ocean models with adjustments to the deep circulation, *J. Phys. Oceanogr.*, *21*, 843–868, 1991.
- Haines, K., Dynamics and data assimilation in oceanography, in *Data Assimilation: Tools for modelling the ocean in a global change perspective*, NATO ASI Ser., Ser. I, vol. 19, edited by P. Brasseur and J. Nihoul, pp. 1–32, Springer-Verlag, New York, 1994.
- Haltiner, G. J., and R. T. Williams, *Numerical Prediction and Dynamic Meteorology*, 477 pp., John Wiley, New York, 1980.
- Holland, W. R., and P. Malanotte-Rizzoli, Assimilation of

- altimeter data into an ocean model: Space versus time resolution studies, *J. Phys. Oceanogr.*, *19*, 1507-1534, 1989.
- Hurlburt, H. E., D. N. Fox, and E. J. Metzger, Statistical inference of weakly correlated subthermocline fields from satellite altimeter data, *J. Geophys. Res.*, *95*, 11,375-11,409, 1990.
- Kalnay, E., et al., The NCEP/NCAR 40-year reanalysis project, *Bull. Am. Meteorol. Soc.*, *77*, 437-471, 1996.
- Levitus, S., Climatological atlas of the world ocean, *NOAA Prof. Pap. No. 13*, 173 pp., U. S. Gov. Print. Off., Washington, D. C., 1982.
- Levitus, S., Annual cycle of temperature and heat storage in the world ocean, *J. Phys. Oceanogr.*, *14*, 727-746, 1984.
- Levitus, S., and T. Boyer, *World Ocean Atlas 1994*, vol. 4, *Temperature*, U. S. Dep. of Comm., Washington, D. C., 1994.
- Mellor, G. L., and T. Ezer, A Gulf Stream model and an altimetry assimilation scheme, *J. Geophys. Res.*, *96*, 8779-8795, 1991.
- Nitani, H., Beginning of the Kuroshio, in *Kuroshio*, edited by H. Stommel and K. Yoshida, pp. 129-163, Univ. of Wash. Press, Seattle, 1972.
- Semtner, A. J., An oceanic general circulation model with bottom topography, *Tech. Rep. 9*, 99 pp., Dep. of Meteorol., Univ. of Calif., Los Angeles, 1974.
- Shaw, P.-T., The intrusion of water masses into the sea southwest of Taiwan, *J. Geophys. Res.*, *94*, 18,213-18,226, 1989.
- Shaw, P.-T., The seasonal variation of the intrusion of the Philippine Sea water into the South China Sea, *J. Geophys. Res.*, *96*, 821-827, 1991.
- Shaw, P.-T., and S.-Y. Chao, Surface circulation in the South China Sea, *Deep Sea Res., Part I*, *41*, 1663-1683, 1994.
- Shaw, P.-T., S.-Y. Chao, K.-K. Liu, S.-C. Pai and C.-T. Liu, Winter upwelling off Luzon in the northeastern South China Sea, *J. Geophys. Res.*, *101*, 16,435-16,448, 1996.
- Shaw, P.-T., S.-Y. Chao, and L.-L. Fu, Sea surface height variations in the South China Sea from satellite altimetry, *Oceanol. Acta*, *22*, 1-17, 1999.
- Smedstad, O. M., and D. N. Fox, Assimilation of altimeter data in a two-layer primitive equation model of the Gulf Stream, *J. Phys. Oceanogr.*, *24*, 305-325, 1994.
- Talagrand, O., and P. Courtier, Variational assimilation of meteorological observations with the adjoint vorticity equation, part I, theory, *Q. J. R. Meteorol. Soc.*, *113*, 1311-1328, 1987.
- Wu, C.-R., P.-T. Shaw, and S.-Y. Chao, Seasonal and inter-annual variations in the velocity field of the South China Sea, *J. Oceanogr.*, *54*, 361-372, 1998.
- Wyrtki, K., Physical oceanography of the southeast Asian waters, in *NAGA Report*, vol. 2, *Scientific Results of Marine Investigation of the South China Sea and the Gulf of Thailand*, 195 pp., Scripps Inst. of Oceanogr., La Jolla, Calif., 1961.
-
- S.-Y. Chao, Horn Point Laboratory, University of Maryland Center for Environmental Science, P. O. Box 775, Cambridge, MD 21613. (e-mail: chao@hpl.umces.edu)
- P.-T. Shaw, Department of Marine, Earth and Atmospheric Sciences, North Carolina State University, Box 8208, Raleigh, NC 27695. (e-mail: pt_shaw@ncsu.edu)
- C.-R. Wu, Center for Ocean and Atmospheric Modeling, Institute of Marine Sciences, University of Southern Mississippi, Building 1103, Room 249, Stennis Space Center, MS 39529. (e-mail: cwu@ssc.usm.edu)

(Received November 25, 1998; revised June 2, 1999; accepted September 9, 1999.)